Chapter 7

Atmospheric Propagation

Radio waves transmitted by satellites propagate mostly through vacuum. At an altitude of roughly 1000 km, they start interacting with the so-called ionosphere, which is a plasma created by the extreme ultraviolet (EUV) component of the solar radiation. This plasma has an influence on radio wave propagation in the altitude range from 80 km to 1000 km. At altitudes above 1000 km the gas and thus the potential electron density are too low for influencing the propagation of the electromagnetic waves significantly. At lower altitude the radiation flux decreases, since the radiation has been absorbed by the molecules, atoms, and ions at higher altitudes. The mean free path of the electrons also diminishes due to the higher gas density, which increases the capture rate and thus induces a further reduction of the density of free electrons. The maximum density is reached in the F-Layer(s) at an altitude between 250 and 400 km. Below 80 km the radiation still causes the dissociation of molecules such as $O_2 \rightarrow O + O$, but its energy is not sufficient for creating a significant population of free electrons. The further propagation in lower layers (mesosphere, stratosphere, and troposphere) takes place in a gas, which successively changes its composition, density, and temperature. The highest density is reached in the troposphere, which contains 90% of the gas and which is the only layer with a significant amount of water vapor. The linear decrease of temperature in the troposphere (around 6.4°/km) implies that water condensates and freezes, and strongly suppresses the water vapor concentration above the troposphere.

Wave propagation in the vacuum is described by the equation:

$$\frac{1}{v^2}\frac{\partial^2}{\partial t^2}\Phi(\vec{x},t) - \Delta\Phi(\vec{x},t) = 0, \tag{7.1}$$

with $\Phi(\vec{x},t)$ being any of the components of the electromagnetic field, with $v = c$ being the velocity of electromagnetic wave in vacuum, and with Δ denoting the Laplace operator:

$$\Delta = \frac{\partial^2}{\partial x^2} + \frac{\partial^2}{\partial y^2} + \frac{\partial^2}{\partial z^2}$$

Equation (7.1) is itself a consequence of Maxwell's equation in vacuum. If the wave enters an area, which contains charged particles, like a plasma or a gas, it starts interacting with it. In classical terms, the wave polarizes the matter, and the polarized matter radiates wave components that superpose with the incident wave. In the microscopic quantum mechanical world, the photons excite electronic states in the atoms, molecules or ions. These states are typically unstable and lead to the re-emission of photons shortly after excitation. In the case of the L-band, there are no significant electronic transitions for the atoms and molecules. For this reason the interaction is weak and only significant in the lower dense part of the atmosphere. In the ionosphere, some electrons are nearly free, they are accelerated in the incident electromagnetic field and radiate as a consequence of this acceleration.

The above processes make it plausible that propagation in a medium such as a gas or plasma is associated with a delay and thus a phase shift of the incident wave. Let ℓ be the length of propagation through the medium, then the duration of propagation in vacuum would be $\tau = \ell/c$. The above processes cause an extra delay $\Delta\tau$ proportional to ℓ, i.e. $\Delta\tau = \alpha\ell$. Observations show that the interaction is rather weak and that $\Delta\tau \ll \tau$, i.e. $\alpha c \ll 1$. This leads to an effective velocity in the medium equal to:

$$v = \frac{\ell}{\tau + \Delta\tau} = c(1 - \alpha + \ldots).$$

These arguments can be made rigorous using Maxwell's equation under the assumption of a linear relationship between the electric field $\vec{E}$, the electric displacement $\vec{D}$, as well as the magnetic induction $\vec{B}$ and the magnetic field $\vec{H}$:

$$\vec{D} = \epsilon\vec{E} \qquad \vec{B} = \mu\vec{H}. \tag{7.2}$$

The parameters ϵ and μ are constants that depend on the medium considered. They are called dielectric constant and magnetic permeability, respectively. The latter is essentially equal to 1 in non-ferromagnetic materials. After substitution of the above relationships, Mawell's equation have a similar form as in vacuum but with different parameters in the equations. A similar wave equation as described by Equation (7.1) can be derived from these modified Maxwell equations. The only change is a modified value of v :

$$v = \frac{c}{\sqrt{\epsilon\mu}}, \tag{7.3}$$

The ratio

$$n = \frac{c}{v}$$

is called refractive index . It plays an important role in the description of atmospheric propagation. Using Equation (7.3), n can also be expressed in the form ($\mu \sim 1$):

$$n = \sqrt{\epsilon}. \tag{7.4}$$

The refractive index bears its name from the refraction at the interface of two media. Snell's law says that the angles α_1 and α_2 at the interface of two media with refractive indices n_1 and n_2 are related by (see Figure 9.15):

$$n_1 \sin\alpha_1 = n_2 \sin\alpha_2 \tag{7.5}$$

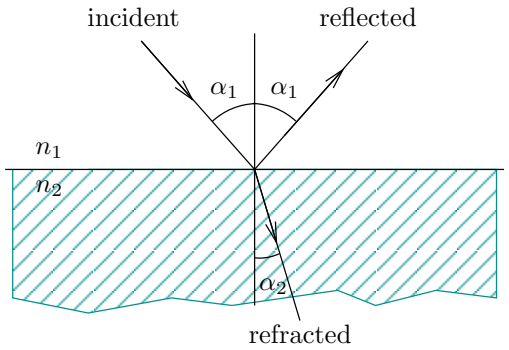

Figure 7.1: Snell's law describes the refraction at the interface of two media. The drawing is valid for $n_1 < n_2$.

For navigation, refraction is a second order effect. It is taken into account in rare cases as a higher order correction. The more important consequence of $n \neq 1$ for navigation is the excess delay due to the modified effective propagation velocity $v \neq c$. The total delay becomes

$$\Delta\tau = \frac{1}{c}\int_{\gamma} d\ell\, n(\ell),$$

with γ being the path taken by the electromagnetic radiation between the satellite and the receiver.

While the above discussion started with the wave nature of electromagnetic radiation, the illustration of Snell's law suggests a ray type propagation, also called geometric optics for the frequencies in the optical domain. It applies whenever the wavelength is much smaller than the scale over which the medium changes significantly. At the macroscopic level, the rays, i.e. the propagation paths, are obtained by Fermat's principle, which states that the radiation takes the path, which leads to an extremal propagation time. In vacuum, this is a straight line. Fermat's principle is fundamental to geometric optics. Snell's law is one of its consequences. Refraction is present in both ionospheric and tropospheric propagation.

7.1 Ionospheric Propagation

The ionosphere is a gas of partially ionized molecules, called plasma. It was described above to be concentrated at altitudes below 1000 km. A plasma of reduced density is also present above that height. It mostly consists of particles from the solar wind that are trapped in the magnetic field of the earth. The role of the geomagnetic field explains the name "Magnetosphere" for this plasma. It extends to roughly 10 times the radius of the earth. The magnetosphere includes the inner van Allan belt, discovered by Explorer I in January 1958. The density of electrons in the magnetosphere is typically too low for influencing propagation delay directly. Its coupling with the ionosphere, however, leads to an indirect influence. Figure 7.2 shows the electron density in near earth space.

In the case that $n_1 > n_2$, Snell's law implied that there is no real-valued solution for $\alpha_1 > \arcsin(n_2/n_1)$. People diving in water observe this phenomenon in the optical domain, and call it total reflection. The same phenomenon also occurs at RF frequencies between 1 MHz to 30 MHz at the F-layer of the ionosphere. It was and is used for communicating over large distances often with several reflections between the ionosphere and the ground. Marconi received the Nobel Prize in 1909 for his transatlantic transmission experiment. He shared the prize with Braun. The existence of the ionosphere was first proposed by Heaviside in 1902. Appleton received the Nobel Prize in 1947 for his investigations of the physics of the ionosphere.

The level of ionization in the ionosphere changes as a function of day-time, the seasons, and solar activity. The orbital movement causes a variable exposition of the southern and northern hemisphere to solar radiation as a function of seasons. The rotation of the earth around its axis leads to a diurnal variation with a maximum of the ionization around 14:00 hours (2 p.m.). The latter variation is shown in Figure 7.4. The solar activity is a stochastic process. Its average shows an 11 year cycle, as can be seen in Figure 7.5. The physics of this cycle are not well understood. The cycle was disrupted for approximately 50 years in the early 17th century. This period is coincident with the small ice age observed in Europe.

7.1.1 Group and Phase Velocity - Dispersion

Since the electrons have a distinct charge and mass, their reaction to electromagnetic waves depends on the frequency of the wave. This frequency dependency has a number of implications:

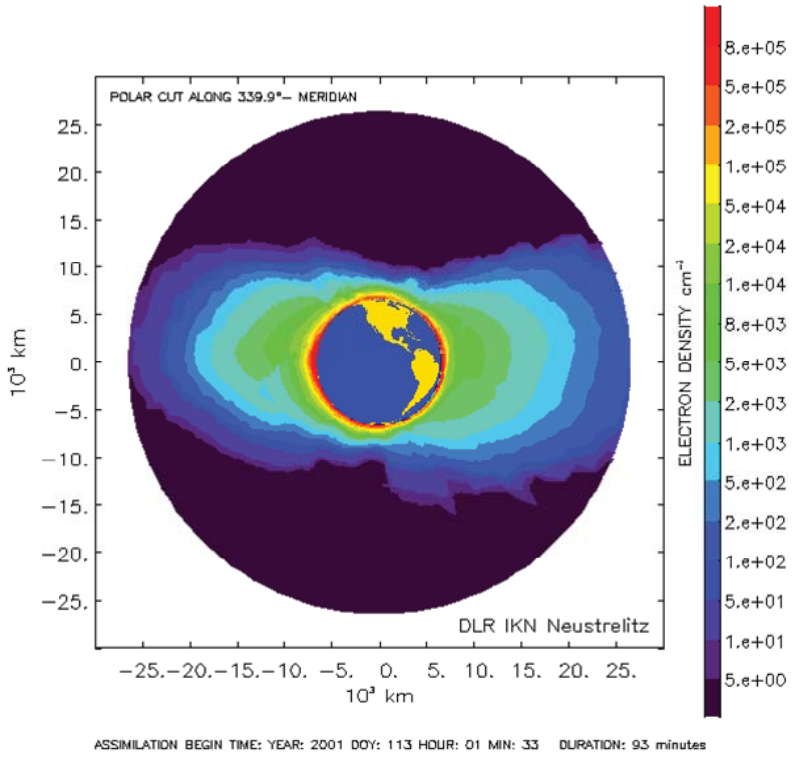

Figure 7.2: Map of the electron density obtained from GPS measurements from the ground and from the LEO orbiting satellite CHAMP. [Courtesy: N. Jakowski, DLR]

- it leads to a different velocity for the modulation and the phase of the signal,
- it allows for the determination of the so-called Total Electron Content (TEC) using measurements at different frequencies, and
- it implies a distortion of the signals, more precisely a broadening of an incident pulse. This is the reason for the name dispersion.

The distortion of signals modulated on carriers in the L-band started only to be considered recently. Christie and Parkinson proposed its use for determining the TEC [1]. Gao, Datta-Barua, Walter, and Enge [2] studied its impact on wideband signals, and Henkel, Gao, Walter, and Günther [3] developed a method for estimating the associated phase error.

The present section focuses on understanding propagation in a dispersive medium. In an isotropic medium, the wave equation can be written in the form:

$$\left(\frac{\partial^2}{\partial t^2} - v^2\Delta\right)\phi(\vec{x},t) = 0, \tag{7.6}$$

with v being the velocity of propagation of the electromagnetic wave in the medium. This equation has the general solution:

$$\phi(\vec{x},t) = f(\vec{x} - \vec{v}t), \tag{7.7}$$

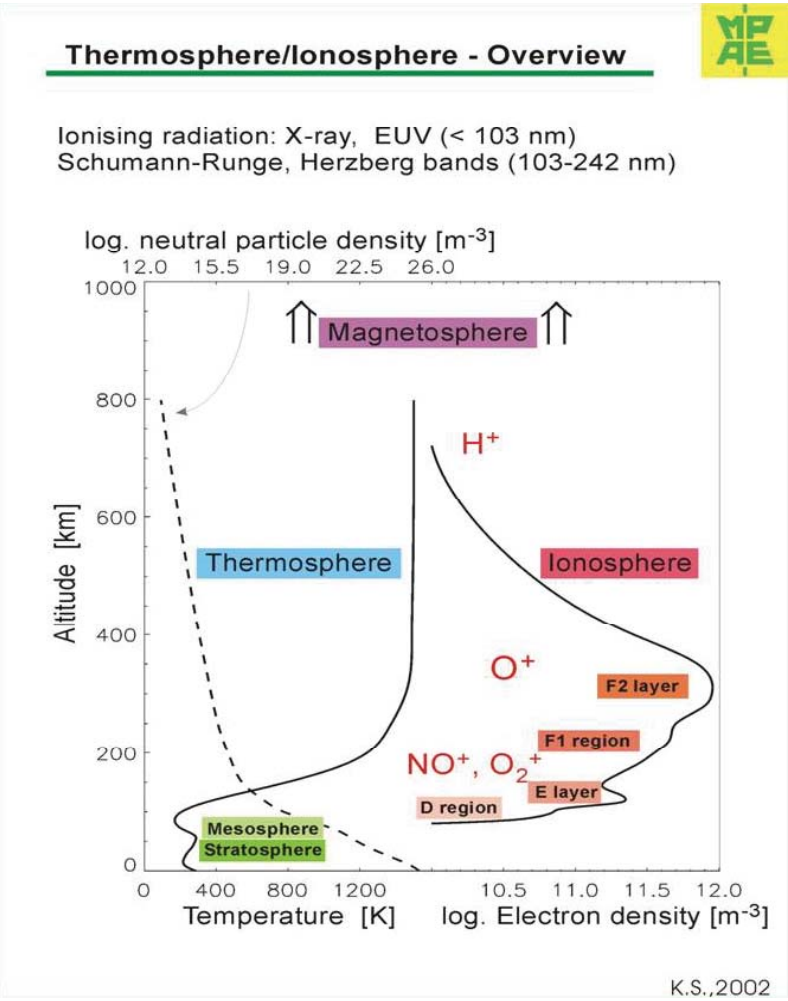

Figure 7.3: Plot of the ionization, the density of neutral particles, and the temperature in the atmosphere. [Courtesy: K. Schlegel, Max Planck Inst. für Aeronomie]

with $f(.)$ being an arbitrary function, $\vec{v} = v\vec{e}$ being the velocity of the wave and $\vec{e}$ being the (arbitrary) direction of propagation. The function

$$f(\vec{x} - \vec{v}t) = e^{j\vec{k}^T(\vec{x}-\vec{v}t)} = e^{j(\vec{k}^T\vec{x}-\omega t)}$$

with

$$\omega = \vec{k}^T\vec{v}$$

is a plane wave solution, i.e. a particular solution. The parameter $\vec{k}$ is called wave number and its i-th component is defined by

$$k_i = \frac{2\pi}{\lambda_i},$$

with λ being the wavelength in that direction. The norm of $\vec{k}$ is denoted by $k = \|\vec{k}\|$. The wave number describes both the spatial angular frequency and the direction of propagation. The location

$$\vec{x} = \vec{x}_0 + \frac{\omega\vec{k}}{k^2}t$$

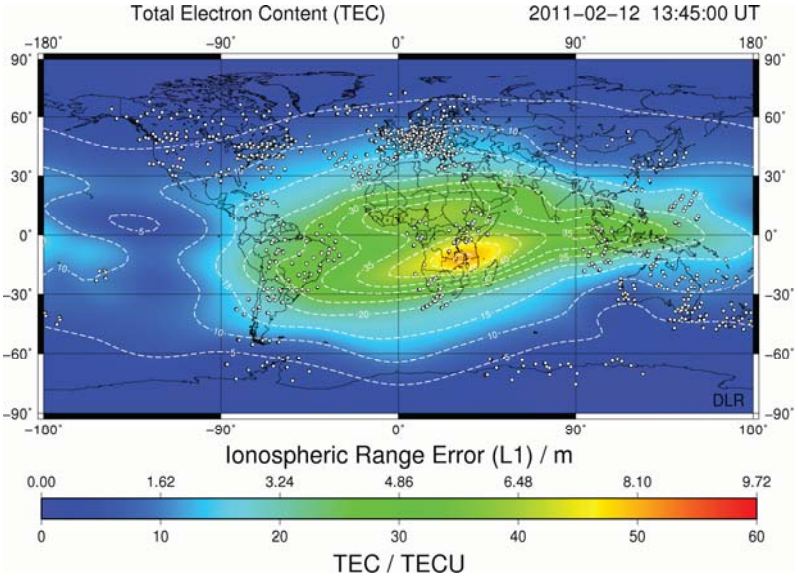

Figure 7.4: Map of the excess delay caused by the ionosphere as a function of time and latitude at 13:45 UT in February. The maximum is in the southern hemisphere. The dot show the ionospheric pierce points of the rays from the satellites to the receivers. [Courtesy: N. Jakoswki, DLR]

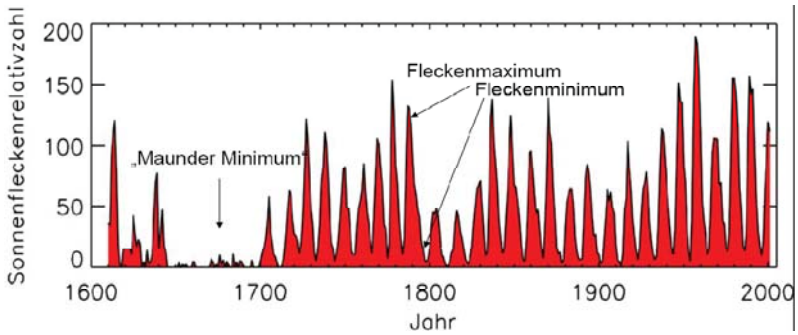

Figure 7.5: Sun spots are a measure of the solar activity. The figure shows the 11 year cycle. [Courtesy: V. Bothmer, Univ. Göttingen]

at time t has the same phase as the location $\vec{x}_0$ at time 0. Thus, it is reasonable to interpret the quantity

$$\vec{v}_{\rm ph} = \frac{\omega \vec{k}}{k^2} \tag{7.8}$$

as being the phase velocity of the wave. Since the velocity v in Equation (7.6) is due to the scattering of the incident wave by atoms and molecules in the gas or plasma, and since these atoms and molecules will respond differently to waves with different spatial frequencies, the velocity v will typically be a function of the wave vector of the incident wave:

$$v = v(\vec{k}).$$

A medium is called dispersive at a certain frequency if a non-trivial functional relation exists and non-dispersive, when $v(\vec{k})$ does not depend on $\vec{k}$, i.e. $\omega(\vec{k}) = ck$, and $v = c$.

The initial conditions for a more general solution can be represented by a Fourier integral:

$$\Phi(\vec{x},0) = \int_{\mathbb{R}^3} d^3q\, F(\vec{q}) e^{j(\vec{k}+\vec{q})^T\vec{x}} = e^{j\vec{k}^T\vec{x}}\Psi(\vec{x}),$$

with $F(\vec{q})$ having appropriate decay properties, and being nearly zero for $|\vec{q}| > Q$. The propagated solution associated with the above initial conditions becomes a superposition of propagated plane waves:

$$\Phi(\vec{x},t) = \int_{\mathbb{R}^3} d^3q\, F(\vec{q}) e^{j((\vec{k}+\vec{q})^T\vec{x}-\omega(\vec{k}+\vec{q})t)}. \tag{7.9}$$

This applies for $v(\vec{k}) = v$, i.e. v independent of $\vec{k}$. In the more general case of a non-constant v, the expression in Equation (7.9) is no more a solution of Equation (7.6), which is not very surprising, since the wave propagates through a medium. The field can induce both electric charges and currents in the medium. The "solution" $\Phi(\vec{x},t)$ described by Equation (7.9) is a phenomenological description of the field in that medium.

In the case of a initial distribution $F(.)$ concentrated around the wave vector $\vec{0}$, it is meaningful to develop the dispersion relation:

$$\omega(\vec{k}+\vec{q}) = \omega(\vec{k}) + \vec{q}^{\,T}\left.\frac{\partial\omega}{\partial\vec{q}}\right|_{\vec{q}=\vec{k}} + \frac{1}{2}\sum_{i,j} q_i M_{ij} q_j \ldots,$$

with

$$M_{ij} = \left.\frac{\partial^2\omega}{\partial q_i \partial q_j}\right|_{\vec{q}=\vec{k}}.$$

Terminating the expansion after the second term is justified by the decay properties of $F(.)$. It implies:

$$\begin{aligned}
\Phi(\vec{x},t) &= e^{j(\vec{k}^T\vec{x}-\omega(\vec{k})t)} \int_{\mathbb{R}^3} d^3q\, F(\vec{q})\, e^{-\frac{1}{2}\vec{q}^T M\vec{q}t}\, e^{j\vec{q}^T(\vec{x}-\left.\frac{\partial\omega}{\partial\vec{q}}\right|_{\vec{k}}t)} && (7.10)\\
&= e^{j(\vec{k}^T\vec{x}-\omega(\vec{k})t)} \int_{\mathbb{R}^3} d^3y\, \frac{1}{(2\pi t)^{3/2}\sqrt{\det M}}\, e^{-\frac{1}{2}\vec{y}^T(tM)^{-1}\vec{y}}\, \Psi(\vec{x}-\left.\frac{\partial\omega}{\partial\vec{q}}\right|_{\vec{k}} t-\vec{y}) && (7.11)
\end{aligned}$$

In the case, that M is non-zero, and M^{-1} non-singular, the convolution implies that the distribution $\Psi(.)$ decays with a standard deviation that increases like $\sqrt{t}$. At the other extreme, if the curvature of the dispersion relation is negligible $\|M\| \ll 1$ or if the pulse is extremely narrowband $Q \ll 1$, the above expression can be approximated by

$$\Phi(\vec{x},t) = e^{j(\vec{k}^T\vec{x}-\omega(\vec{k})t)}\Psi(\vec{x}-\left.\frac{\partial\omega}{\partial\vec{q}}\right|_{\vec{k}} t),$$

This is the equation of a wave, which propagates with the phase velocity (see Equation (7.8)):

$$\vec{v}_{\rm ph} = \frac{\omega(\vec{k})\vec{k}}{k^2}, \tag{7.12}$$

and a modulation, which propagates with the group velocity

$$\vec{v}_{\rm gr} = \left.\frac{\partial\omega(\vec{q})}{\partial\vec{q}}\right|_{\vec{q}=\vec{k}}. \tag{7.13}$$

If some eigenvalues of M are zero, while others are not, diffusion only takes place in the direction of non-zero eigenvalues. Equation (7.12) implies that

$$v_{\rm ph} = \frac{\omega(\vec{k})}{k}, \quad \text{and} \quad \vec{e} = \frac{\vec{k}}{k},$$

and with the assumption of isotropy, i.e. that $v(\vec{k}) = v(k)$, also that

$$\omega(\vec{k}) = \omega(k).$$

As a consequence, one has

$$\vec{v}_{\rm gr} = \frac{\partial\omega(q)}{\partial q}\frac{\partial q}{\partial\vec{q}}\bigg|_{\vec{q}=\vec{k}} = \frac{d\omega(q)}{dq}\bigg|_{q=k}\vec{e},$$

and thus the definition of

$$v_{\rm gr} = \frac{d\omega(q)}{dq}\bigg|_{q=k}.$$

The above discussion suggests three grades of dispersion:

- No dispersion at all:

  $$v_{\rm gr} = v_{\rm ph} = v.$$

  This applies to the propagation of L-band signals through the troposphere.

- Weak dispersion with a group velocity, given by Equation (7.13), different from the phase velocity but with a negligible distortion of the waveform. This is the typical case for propagation through the ionosphere at L-band frequencies.

- Strong dispersion with a deformation of the waveform given by Equation (7.10). Such deformations need only to be taken into account in precision applications, which use Galileo ALTBOC signals[1].

Both velocities lead to the definition of individual refraction indices:

$$n_{\rm ph} = \frac{c}{v_{\rm ph}}, \qquad n_{\rm gr} = \frac{c}{v_{\rm gr}}, \tag{7.14}$$

which are related through the following equation:

$$\begin{aligned} n_{\rm gr} &= n_{\rm ph} + \omega\frac{dn_{\rm ph}}{d\omega} \\ &= n_{\rm ph} + f\frac{dn_{\rm ph}}{df}, \end{aligned} \tag{7.15}$$

as can be verified by using the definition of $v_{\rm ph}$ and $v_{\rm gr}$.

7.1.2 First Order Ionospheric Delay

As mentioned already an incident wave polarizes the plasma. Due to the mass ratio of more than 1000 between the electrons and the nuclei, the electrons are the primary source of polarization. The polarization $\vec{P}$ is proportional to the strength of the incident field and to the electron density n_e:

$$\vec{P} = \alpha\, n_e\vec{E}. \tag{7.16}$$

The identity

$$-{\rm div}\vec{P} = \rho$$

- derived from the definition of the polarization as the dipole moment per unit volume - and a corresponding relation between the magnetization and the currents (including dielectric displacement), allow for a reformulation of Maxwell's equation in terms of the fields $\vec{E}, \vec{D}, \vec{H}$, and $\vec{B}$. The

[1]The impact on split spectrum signals such as those obtained from BOC- or ALTBOC-modulation is more pronounced than for PSK modulated signals since the power of the former signals is more widely spread in frequency.

electric displacement field $\vec{D}$ introduced in this reformulation is defined as the superposition of the external field $\vec{E}$ and the field induced by the polarization:

$$\vec{D} = \vec{E} + 4\pi\vec{P}.$$

Together with the assumptions of Equation (7.2) and Equation (7.4) this implies

$$n^2 = 1 + 4\pi\alpha n_e.$$

The simplest model for α describes the electrons as being classical particles accelerated by the electric field of a plane incident electromagnetic wave $\vec{E}(\vec{x},t) = \vec{E}_0 e^{j(\vec{k}\vec{x}-\omega t)}$:

$$m\ddot{\vec{\xi}} = e\vec{E}_0 e^{j(\vec{k}\vec{x}-\omega t)}.$$

If one neglects transient phenomena, this equation has the solution

$$\vec{\xi} = -\frac{e}{m\omega^2}\vec{E}.$$

With $\vec{p} = e\vec{\xi}$, the dipole moment generated by a single electron, the polarization becomes

$$\vec{P} = n_e\, e\vec{\xi} = -n_e \frac{e^2}{m\omega^2}\vec{E},$$

which together with Equation (7.16) implies that:

$$\alpha = -\frac{e^2}{m\omega^2}.$$

This suggests the following model for the ionospheric refraction index n_{ph} of first order:

$$\begin{aligned} n_{\mathrm{ph}}(f) &= \sqrt{1 - 4\pi\frac{e^2}{m}\frac{n_e}{\omega^2}} && (7.17)\\ &\simeq 1 - 2\pi\frac{e^2}{m}\frac{n_e}{\omega^2} && (7.18)\\ &= 1 - \frac{40.3 n_e}{f^2}, && (7.19) \end{aligned}$$

with the numerical value being valid if the electron density n_e is measured in $[\mathrm{m}^{-3}]$. The corresponding model for the group refractive index is derived from Equation (7.14) to be:

$$n_{\mathrm{gr}}(f) = 1 + \frac{40.3 n_e}{f^2}, \tag{7.20}$$

This immediately implies that the excess delay for the phase I_{ph} and the modulation I_{gr} are exactly opposite:

$$I_{\mathrm{gr}} = \frac{1}{c}\int_\gamma d\ell\,(n_{\mathrm{gr}}(\ell) - 1) = -I_{\mathrm{ph}} \geq 0.$$

The ionosphere thus causes a phase advance ($I_{\mathrm{ph}} \leq 0$) and a group delay ($I_{\mathrm{gr}} \geq 0$). The latter delay is relevant to code measurements, i.e. the modulation. The former advancement described the impact on phase measurements.

Both delays do not depend on the detailed electron density distribution but only on the integral

$$\int_\gamma d\ell\, n_e(\ell),$$

which is called Total Electron Content (TEC). The unit is the TEC Unit (TECU), which corresponds to 10^{16} electrons/m^2. At the frequency 1575.42 MHz (L1), one TECU implies a range error of 16.3 cm.

In the case of multi-frequency receivers the ionospheric delay can be eliminated. Its determination can be based on code or phase measurements, as well as on a combination of both. The phase measurement of the ionosphere is much less noisy but ambiguous. Different techniques for handling the ambiguity are described in Chapter 16. It is left as an exercise to determine the appropriate linear combination.

7.1.3 Second Order Ionospheric Corrections

In the case of high accuracy applications, second order corrections must be considered. They are no more isotropic, but rather depend on the direction of the magnetic field at the location of the plasma. The size of these corrections can reach a few centimeters, as reported by Hoque and Jakowski [7].

The second order corrections were derived by Bassiri and Hajj [8] from the magnetohydrodynamic equations. Let J and J_φ denote the 2nd order corrections to the code and phase measurements, respectively, then:

$$J = \frac{s}{f^3} \tag{7.21}$$

$$J_\varphi = -\frac{1}{2}J, \tag{7.22}$$

with

$$s = 7527\, c \int_\gamma d\ell\, n_e(\ell)\, \vec{B}(\ell) \cdot \vec{e}(\ell),$$

and c denoting the velocity of light, n_e the electron density, $\vec{B}$ the earth magnetic field, and $\vec{e} = \vec{k}/\|\vec{k}\|$ the unit vector in the direction of wave propagation. The latter is typically approximated by the unit vector pointing from the satellite to the user location, i.e., $\vec{e}(\ell) = \vec{e}$ or said differently ray bending is neglected. In this case, s can also be written in the form

$$s = \vec{s} \cdot \vec{e}.$$

The vector delay $\vec{s}$ needs to be mapped in a similar manner as the TEC in the single frequency case.

7.1.4 Mapping Function - Ionospheric Delay

In the previous section, the characterization of the ionosphere could be reduced to a single number - the TEC - for every conceivable path. This still implies a considerable complexity, if one wishes to describe the ionosphere for all possible receiver locations. The following simplified geometric model reduces the complexity significantly.

As mentioned already, the electron density is significant between 80 and 1000 km, with the highest density somewhere between 250 and 400 km. The reference height h in the following discussion is thus chosen to be $h = 350$ km. The ionosphere is modeled as a shell around $R_e + h$. This shell can be considered as being locally flat, because its thickness is much smaller than R_e. The path from the satellite to the receiver crosses the height $R_e + h$ in a point with latitude λ_I and longitude ϕ_I, called the Ionospheric Pierce Point (IPP). The path crosses the shell with an angle ζ' measured from the zenith direction. Define the vertical TEC (TECV) as being the TEC observed by a receiver, directly located under the piercing point, then the two values are related by

$$\text{TECV} = \text{TEC} \cdot \cos\zeta'.$$

This is a consequence of the geometry shown in Figure 7.6. TECV is assumed to be independent of ζ', which is fulfilled whenever the ionosphere is sufficiently homogeneous and isotropic on every spherical shell. The angle ζ' is related to the zenith angle of the satellite $\zeta = \pi/2 - E$ or the elevation E at the receiver location by applying the law of sines:

$$\frac{\sin\zeta'}{R_e} = \frac{\sin(\pi-\zeta)}{R_e+h} = \frac{\sin\zeta}{R_e+h}.$$

Thus, knowing TECV allows to determine TEC(ζ) through:

$$\mathrm{TEC}(\zeta) = \frac{\mathrm{TECV}}{\cos\zeta'} = \frac{\mathrm{TECV}}{\sqrt{1-\dfrac{\sin^2\zeta}{(1+h/R_e)^2}}}. \tag{7.23}$$

The multiplier of TECV is sometimes called obliquity factor or mapping function. It is then denoted by $m_I(E)$. Since satellites are not used below an elevation of 5°, this factor is between 1 and 3.04. The values of the vertical TEC can be derived from map services associated with augmentation systems such as WAAS and EGNOS or as provided by DLR. In all these cases, the TECV values are delivered for a discrete grid. The values for the actual piercing points must be interpolated. Alternatively, these values can also be obtained from models as described in the next section.

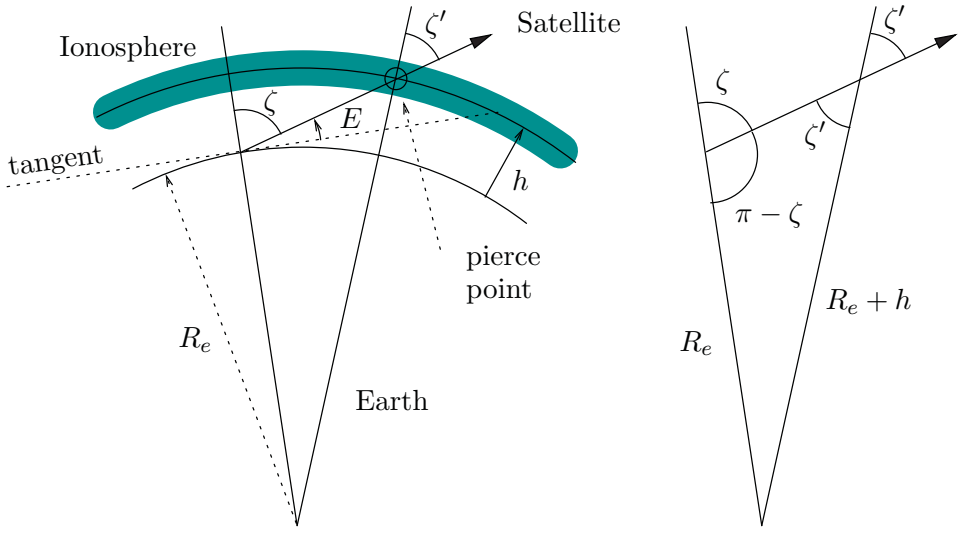

Figure 7.6: Geometry of ionospheric propagation. The TEC and TECV are related by geometry if the ionosphere is sufficiently homogeneous.

7.1.5 Klobuchar Model

The Klobuchar model [4] is a simple and rather effective model for TECV. It is capable of eliminating 50-60% of the ionospheric excess delay under nominal conditions, i.e. outside storm periods. This model is used in GPS, its parameters are included in the navigation message [5]. They describe the ionospheric delay at L1 frequency, i.e. 1575.42 MHz.

The daily variation of the ionosphere is described by a truncated and offset cosine function (see Figure 7.7):

$$I = \begin{cases} A_1 + A_2 \cos\left(\frac{2\pi(t-A_3)}{A_4}\right) & \text{if } |t - A_3| < \frac{A_4}{4} \\ A_1 & \text{otherwise.} \end{cases}$$

The cosine function describes the angular dependency of the power flux on a horizontal surface, which is used as a simplified description for the angle in three dimensions. In the case of the ionosphere, the function is not centered at noon, however. This is due to the complex response of the ionosphere to solar radiation. The above function has four parameters. Two of them are modeled as being constant and two are described by coefficients in the navigation message:

- $A_1 = 5 \cdot 10^{-9}$ [s], is the constant value during night time,
- $A_2 = \sum_{n=0}^{3} \alpha_n \phi_m^n$ is the maximum amplitude during daytime. It is described by a polynomial in the *geomagnetic latitude* ϕ_m. The coefficients α_n of the polynomial are included in the navigation message. They depend on the current solar activity.
- $A_3 = 50400$ [s] $= 14$ [h] is the constant value of the daily maximum, with t measured in local solar time. This value is a model constant.
- $A_4 = \sum_{n=0}^{3} \beta_n \phi_m^n$ is another polynomial describing the period of the cosine. It is also supplied in the navigation message.

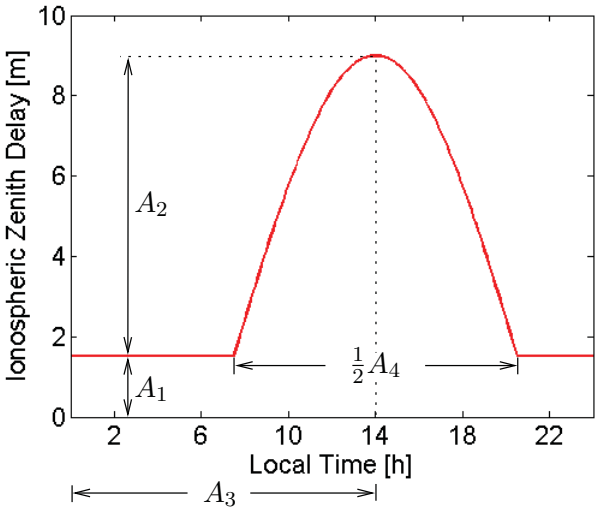

Figure 7.7: The daily variation of the TECV is characterized by four parameters $A_1 - A_4$.

The prediction of the Klobuchar model can be related to the measurements shown in Figure 7.3. The distribution is mostly symmetric around 14 h, and the constant night value is at roughly 1.5 m. The exact model, as specified by Klobuchar and in the GPS ICD, deviates slightly from the above description by using polynomial approximations of the trigonometric functions.

The Galileo system has adopted a different ionospheric model, called NeQuick, see [9] for its most recent variant. This model is a three-dimensional model with a very large number of coefficients (more than 1000, which must be updated every few years, due to the change in the earth's magnetic field), and three solar activity parameter. The performance of the model is improved as compared to the Klobuchar-Model in the case of increased solar activity (see Figure 7.9).

7.2 JHM-Model

Jakowski, Hoque, and Mayer have recently developed an alternative model [6]. Like the Klobuchar model, it is a phenomenological model, which describes the average behavior of a nominal ionosphere. The situation under storm conditions can be rather different. The model has a bias of 0.3 TECU and a root mean square deviation of 7.5 TECU, which is similar to NeQuick. The advantage of JHM over NeQuick is its great simplicity. It only includes 19 fixed coefficients and one variable parameter. The latter is the solar flux F10.7 at 2880 MHz[2]. It is measured directly on the surface of the earth, using a medium size reflector, and an appropriate calibration. The vertical TECV in the JHM-model is represented as a product of factors, which describe the dependency on: hour angle[3] h and declination δ of the sun; on the latitude ϕ and geomagnetic latitude ϕ_m of the pierce point; as well as on the season[4] $t \bmod y$ and the solar activity (F10.7):

$$\mathrm{TECV} = F_1(h, \delta, \phi) \cdot F_2(t \bmod y) \cdot F_3(\phi_m) \cdot F_4(\phi_m) \cdot F_5(\mathrm{F10.7}). \tag{7.24}$$

The description of these terms fully specify the model. Some constants were determined by intuition, others are the result of a least-squares fit. The latter ones are summarized in Table 7.1. The former ones are directly described in the text.

The last term in Equation (7.24) describes the relation between the solar flux F10.7 and its impact on ionospheric delay. The relation is linear:

$$F_5(\mathrm{F10.7}) = c_{11} + c_{12}\,\mathrm{F10.7}.$$

F10.7 istelf is expressed in surface flux units (sfu):

$$1\ [\mathrm{sfu}] = 10^{-22}\mathrm{Wm}^{-2}\mathrm{Hz}^{-1}.$$

Typical values for a nominal ionosphere are between 70 and 200. The value during storms can reach 400. The units of c_{11} and c_{12} are TECU and TECU/sfu, respectively. All other coefficients c_i below are numbers without units.

The coupling of the solar wind into the magnetosphere and ionosphere depends on the orientation of the earth axis, which changes as a function of seasons. This is described by

$$F_2(t \bmod y) = 1 + c_6 \cos\left(2\pi \frac{t - t_A}{y}\right) + c_7 \cos\left(4\pi \frac{t - t_{SA}}{y}\right) \tag{7.25}$$

with t being the local solar time[5], and with $t_A = 18$ days and $t_{SA} = 6$ days being an annual and semi-annual offset. Equation (7.25) describes the first three terms of a Fourier series. The odd terms in the series have been absorbed in the annual and semi-annual offsets. The magnetohydrodynamics of the ionosphere causes an irregular distribution of the electron density, which is described by a symmetric term:

$$F_3(\phi_m) = 1 + c_8 \cos \phi_m,$$

and two equatorial anomaly crest terms:

$$F_4(\phi_m) = 1 + c_9 e^{-\frac{(\phi_m - \phi_{c_N})}{2\sigma^2_{c_N}}} + c_{10} e^{-\frac{(\phi_m - \phi_{c_S})}{2\sigma^2_{c_S}}}$$

with the following offsets and standard deviations of the crests: $\phi_{c_N} = 16°\mathrm{N}$, $\sigma_{c_N} = 12°$, and $\phi_{c_S} = 10°\mathrm{S}$, $\sigma_{c_S} = 13°$. The last term to be described is the variation of TECV as a function of the hour angle h of the sun, which is presently equal to

$$h = t \bmod d + \frac{d}{2},$$

[2]This corresponds to a wavelength of 10.7 centimeters.

[3]The hour angle is the angle in the equatorial plane between a celestial body (presently the sun) and an observer (presently the ionospheric pierce point). It is positive when the body is in the west of the observer.

[4]y is the duration of a mean sidereal year, which is approximately 365.25 d.

[5]Using the sidereal time would be more logical, but would hardly make a difference.

Coefficient	Estimated Value	α
c_1	0.89656	0.001081
c_2	0.16984	0.000985
c_3	-0.02166	0.000965
c_4	0.05928	0.000975
c_5	0.00738	0.000976
c_6	0.13912	0.000652
c_7	-0.17593	0.000615
c_8	-0.34545	0.004341
c_9	1.1167	0.007428
c_{10}	1.1573	0.008330
c_{11}	-4.3356	0.035044
c_{12}	0.17775	0.000596

Table 7.1: Coefficients used in the JHM-Model. The 95% confidence value α is defined to be such that $\int_{-\alpha}^{\alpha} p(a_i = \beta)\, d\beta = 0.95$ [6].

with d being the duration of a solar day. Due to the simplicity of this relationship, the hour angle and time of the day t mod d are used interchangeably. The illumination of a surface element at latitude ϕ by a sun at an hour angle h and a declination δ is proportional to:

$$\cos\theta = \cos\left(\frac{2\pi h}{d}\right)\cos\delta\cos\phi + \sin\delta\sin\phi,$$

whenever the pierce point is on the hemisphere pointing towards the sun. It would be zero in the shadow area, and something in-between for the region that is not shadowed and not lying on the mentioned hemisphere. The reality is more complex, since the plasma also extends into the shadow area. The actual empirical dependency is

$$F_1(t,\phi,\delta) = (0.4 + \cos(\phi-\delta)) + \left(c_1\cos(2\pi\frac{t-t_D}{d}) + c_2'\cos(4\pi\frac{t-t_{SD}'}{d}) + c_4'\cos(6\pi\frac{t-t_{TD}'}{d})\right)\cos\chi,$$

with

$$\cos\chi = \cos(\phi-\delta) - \frac{2\phi}{\pi}\sin\delta.$$

The expression for F_1 again includes a Fourier expansion with sinus-components hidden in a phase-term. Jakowsky, Hoque and Mayer, make two of those components explicit by replacing:

$$c_2'\cos(4\pi\frac{t-t_{SD}'}{d}) + c_4'\cos(6\pi\frac{t-t_{TD}'}{d})$$

by

$$c_2\cos(4\pi\frac{t}{d}) + c_3\sin(4\pi\frac{t}{d}) + c_4\cos(6\pi\frac{t}{d}) + c_5\sin(6\pi\frac{t}{d}).$$

Together with Table 7.1 this fully describes the JHM-model. Figure 7.8 shows the geographic dependency of TECV as predicetd by the JHM-model for a particular time instant. Today, there is no further justification for the functional description proposed by Jakowski, Hoque and Mayer than the quality of the fit. The latter is visible from a comparison with data from the measurements using TOPEX/Poseidon, as shown in Figure 7.9. The same plot also shows the performance of Klobuchar and NeQuick.

Figure 7.8: Geographic distribution of TEC from the JHM-Model for F10.7=140 [sfu] at noon in Munich during the Spring equinox [Courtesy N. Jakowsy, M. Hoque, C. Meier, DLR, 2012].

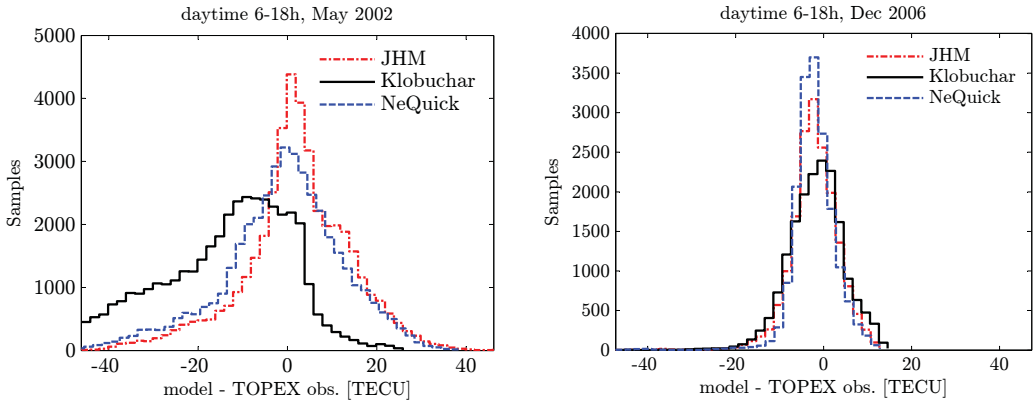

Figure 7.9: Comparison of the error distributions for Klobuchar, NeQuick and the JHM-Model as compared to TOPEX Poseidon Data. The left graph shows a situation where the newer models outperform Klobuchar (see Table 7.2 for the values of the parameters) [Courtesy N. Jakowsy, M. Hoque, C. Meier, DLR, 2012].

7.2.1 Summary - Ionosphere

The ionospheric delay is one of the largest source of uncertainty in satellite navigation. This delay varies substantially during the day. Due to the unpredictability of solar activity and the complexity of magnetohydrodynamics it is difficult to accurately model the TEC under all conditions. Under worst case storm scenarios, zenith delays of up to 36 m have been observed. The nominal ionosphere can be described with a 95% confidence of roughly 1 meter using NeQuick and the JHM-Model. This is sufficient for applications such as car navigation. Early forms of TEX prediction have been developed recently as well. Multi-frequency receivers can accurately estimate the ionospheric delay. Modernized GPS and Galileo are likely to further the use of this option. The estimation capability of multi-frequency signals is a consequence of dispersion, i.e. of the frequency dependency of the refraction index. In this context, scintillations that occur during storms remain a threat. They induce cycle slips and might cause a receiver loosing lock. A substantial effort is being made to predict the occurrence and severity of scintillations.

Data set	Model	rms error	mean error	std dev.
May 2002	JHM	12.5	1.2	12.4
	Klobuchar	22.8	-16	16.2
	NeQuick	13.6	-2	13.5
Dec 2006	JHM	6.4	-3.1	5.6
	Klobuchar	6.9	-2.7	6,4
	NeQuick	5.9	-3.1	5

Table 7.2: The values of the root mean square error, of the error and of the standard deviation of the distribution show the strength of the newer model in the case of increased solar activity (May 2002) [Courtesy N. Jakowsy, M. Hoque, C. Meier, DLR, 2012].

7.3 Tropospheric Propagation

The tropospheric delay denotes the delay caused by the neutral gases in the atmosphere. These gases extend somewhat beyond the boundary of the troposphere at 9-16 km height. Tropospheric propagation is non-dispersive at L-band frequencies, i.e. the group and phase velocities are identical $v < c$. The refraction is comparatively small. The maximum zenith delay is of the order of 2.5 m. This also means that $n \sim 1$. Therefore, the refractivity is introduced:

$$N = 10^6(n-1).$$

The excess delay becomes:

$$\begin{aligned} \Delta\tau &= \frac{1}{c}\int_{\gamma_{\text{em}}} d\ell\, n(\ell) \;-\; \frac{1}{c}\int_{\gamma_{\text{geom}}} d\ell \\ &= \frac{10^{-6}}{c}\int_{\gamma_{\text{em}}} d\ell\, N(\ell) + \frac{1}{c}\int_{\gamma_{\text{em}}-\gamma_{\text{geom}}} d\ell \end{aligned} \tag{7.26}$$

The first term in Equation (7.26) is the excess delay due to the slower propagation on the curved path γ_{em} of the signal. The second term is the delay difference between the curved path and the direct geometric path γ_{geom}. It is neglected due to its marginal impact.

The gases in the troposphere are subdivided into two groups: Water molecules, and other constituents. Some of the latter are listed in Table 7.3. They form the "dry" part, while the water vapor forms the "wet" part. The distinction is motivated by the different thermodynamical and electromagnetic properties. The partial pressure of the wet component varies significantly as a function of time and location. Water can be present in the form of vapor, water droplets and ice crystals. The associated phase transitions contribute to changes in the partial pressure. Fortunately, water vapor only contributes around 10% of the tropospheric delay. The second distinction is that water molecules are the only molecules that have an intrinsic dipole moment. The tropospheric delay is due to the polarization of the gas, and is proportional to the density of gas particles $\nu\mathcal{N}_A/V$, and a coupling constant K_1 dependent on the type of molecules. In this expression $\mathcal{N}_A = 6.022 \cdot 10^{26}$ kmol^{-1} is Avogadro's number, and ν the number of kilomoles contained in the volume V. Furthermore, let p be the pressure of the dry component, and the T the temperature in degree Kelvin, then the ideal gas law $pV = \nu RT$, implies the following expression for the dry component:

$$N_d = K_1\frac{\nu\mathcal{N}_A}{V} = k_1\frac{p}{T}, \tag{7.27}$$

with $k_1 = K_1\mathcal{N}_A/R$, and $R = 8314.34 \pm 0.35$ [J/(°K·kmol)] denoting the gas constant. The water vapor has a similar first term, supplemented by a second term from the orientation of the dipole

Constituent	Molar weight kg/kmol	Fractional Volume	σ
N_2	28.0134	0.78084	0.00004
O_2	31.9988	0.209476	0.00002
Ar	39.948	0.00934	0.00001
CO_2	44.00995	0.000314	0.00001
H_2O	18.01528	-	-

Table 7.3: Most important gases in the atmosphere, the average weight of the isotopes, their fractional volume, as well as the uncertainty of the latter quantity. The weights are from the US Standard Atmosphere 1976 [11], the volumetric quantities from Glueckauf [Source: Davis, Herring, Shapiro, Rogers, and Elgered [18]]. The fractional volume of H_2O is widely varying depending on weather conditions.

k_1 [K/mbar]	k_2 [K/mbar]	k_3 [K^2/mbar]	Source
77.604 ± 0.014	64.79 ± 0.08	$377'600 \pm 400$	Thayer, 1974
	71.4 ± 5.8	$374'700 \pm 2'900$	Birnbaum, Chatterjee, 1952
	72 ± 11	$375'000 \pm 3'000$	Boudouris, 1963

Table 7.4: Refractivity constants, as indicated by Davis, Herring, Shapiro, Rogers, and Elgered [18]. The values of Thayer are extrapolated from the optical region, while the other values are from measurements in the microwave domain. The values of Thayer are usually taken, although the extrapolation is contested.

moment of these molecules:

$$N_w = k_2 \frac{e}{T} + k_3 \frac{e}{T^2}, \tag{7.28}$$

with e denoting the partial pressure of the water vapor. The constants are summarized in Table 7.4. This description of refractivity is due to Thayer [12]. With his expressions, the integral in Equation (7.26) becomes dependent on the pressure and temperature along the integration path. Since the gases are assumed to be ideal, they do not interact, except for a small amount needed to ensure thermodynamic equilibrium and thus an identical temperature. In this situation each gas acts as if it was alone in the given volume, and the partial pressures simply add (Dalton's Law). The proportionality of the refractivity to the pressure thus implies:

$$N = N_d + N_w, \tag{7.29}$$

In order to simplify the notations, the delay $\Delta\tau$ will be mostly written in the form of an excess path length

$$\Delta s = c\Delta\tau,$$

and will thus be expressed in meters. This effective excess path length should not be seen as a geometric detour. Path bending is negligible in most circumstances. Where not ambiguous, this effective excess path length will be called delay.

The partial pressures and temperature can typically be considered as a function of height only - at least locally. The total tropospheric delay then becomes:

$$\Delta s = 10^{-6} \int_{R_0}^{R_s} dr \, \frac{N(r)}{\cos\zeta(r)}, \tag{7.30}$$

and similar expressions for the dry delay $\Delta\tau_d$ and wet delay $\Delta\tau_w$. The variable $\zeta(r)$ denotes the zenith angle of the path at height r, see Figure 7.10. The integration is extended from the satellite

to the user with R_s and R_0 denoting the corresponding radii. In practice, the integration can be limited to a height of 50 km. The residual error from higher layers is smaller than 3 mm [16].

There are two very different approaches to the computation of troposheric delays. The first one uses atmospheric models in order to derive expressions for the pressure and temperature profiles. This is used as a basis for evaluating the integral (7.30) explicitly. The second approach only relates the slant delay, i.e. the delay experienced by a satellite at an elevation E, with the zenith delay:

$$\Delta s = m_d(E)\Delta s_{z,d} + m_w(E)\Delta s_{z,w},$$

with $m_x(E)$ being the mapping functions for the dry $(x=d)$ and wet components $(x=w)$, respectively. Different mapping functions are needed due to the differing profiles of the two components. With these expressions in mind, the zenith delays are then determined as two additional unknown parameters. This approach is more accurate but also implies more complex processing and additional measurements. It is used by IGS, for example.

The mapping function also allows to reduce the consideration of atmospheric models to the computation of zenith delays. Note that the complete discussion did not address any azimuthal dependency. This is justified because the troposphere is comparatively thin. As a consequence, the part of the path through the troposphere is rather localized. The dry component is quite homogeneous anyway. The wet component, which might be less homogeneous, does only contribute with 10%. Such arguments, as well as the difficulty to handle any azimuthal dependency, even if it was present, have led to its disconsideration.

Equation (7.30) depends on the zenith angle $\zeta(r)$ at the distance r from the center of the earth, or at height $h = r - R_e$. The zenith angle at height h must be related to the zenith angle ζ_0 at the user height or equivalently to the satellite elevation $E = \pi/2 - \zeta_0$. The geometry of Figure 7.10 implies:

$$(R_e + h)\sin\zeta = (R_e + h')\sin\tilde{\zeta} = (R_e + h')\frac{n'}{n}\sin\zeta',$$

with the law of sines (1st equality) and Snell's law (2nd equality) being used. In this equation, a discrete interface was assumed at the height h', while no interface was assumed between h and h'. Since the distance between these interfaces can be made arbitrarily small and since the relation effectively reads:

$$(R_e + h)n(h)\sin\zeta(h) = \text{const}, \tag{7.31}$$

it is valid in general. Thus

$$\cos\zeta(h) = \sqrt{1 - \left(\frac{R_0 n_0 \cos E}{(R_e + h)n(h)}\right)^2}, \tag{7.32}$$

with R_0 denoting the user's distance from the earth center and with n_0 denoting the refraction index at his height.

7.3.1 Atmospheric Models

The simpler atmospheric models describe the zenith delay only for $\zeta_0 = 0$, i.e. for $\zeta(h) = 0$. Equation (7.30) then becomes:

$$\Delta s = 10^{-6}\int_{h_0}^{h_s} dh\, N(h), \tag{7.33}$$

and the analysis is reduced to the study of this integral. The main tasks are the determination of the pressure and temperature profiles. Figure 7.12 shows the temperature profile of the lower standard atmosphere, as derived from empirical data and modeling. In the relevant part, this graph shows a constant lapse rate of $-6.5°$K/km. The model is highly simplified. It was used for the determination of barometric height in aeronautics. The assumption of a constant lapse rate

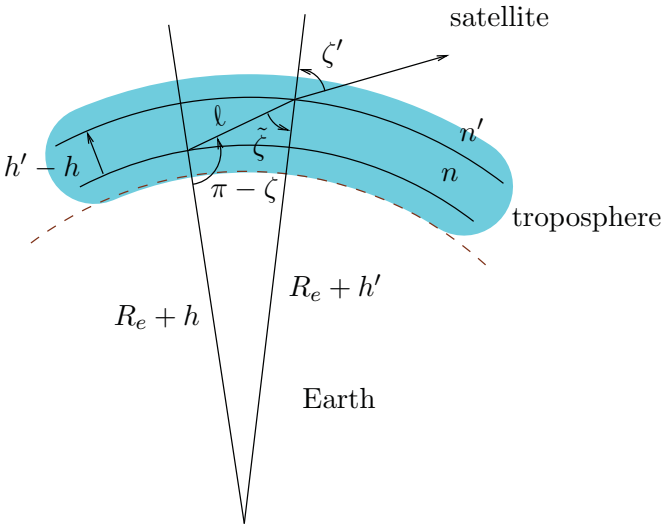

Figure 7.10: Path geometry through the troposphere. The angle ζ' is obtained from the sine law. The angle $\tilde{\zeta}$ follows from Snell's law. The height of the troposphere is exaggerated for visualization purposes.

is equivalent to the assumption of no heat exchange (adiabatic condition), see Appendix A for details. The constant lapse rate was the basis for Hopfield's derivation of a power law dependency of the refractivity on altitude [13].

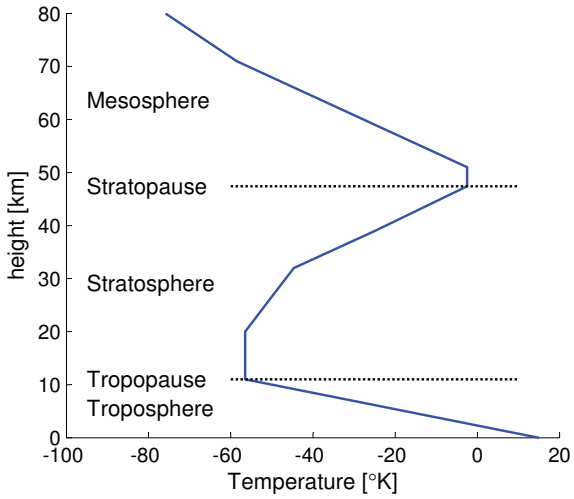

Figure 7.11: Temperature profile for the US Standard Atmosphere 1976 for altitudes up to 80 km. The profiles shows a constant lapse rate of 6.5°/km up to the tropopause, where the temperature first becomes constant, before it starts increasing again above 20 km. [Source [11]]

The atmospheric pressure is build up by gravitation. The volume of air in a box with a base-surface S and height dh has a mass $\rho S\, dh$. It therefore contributes to the force exerted on the gas

volume below it with:

$$dF = S\,dp = -\rho\,g\,S\,dh,$$

which leads to the equation

$$\frac{dp(h)}{dh} = -\rho(h)g(h). \tag{7.34}$$

A power expansion of the gravitational force is justified due to the small altitudes considered ($h \ll R_e$). Simplified models use $g(h) = 9.80665$ [m/s^2]. Saastamoinen introduced a more accurate model, which includes both a dependency on height h as well as on the latitude ϕ for compensating the flattening of the geoid [14]:

$$g(h,\phi) = 97.84 \cdot (1 - 0.00266\cos(2\phi) - 0.00028h) = 97.84 \cdot \gamma(h,\phi), \tag{7.35}$$

with h being measured in kilometers.

Equation (7.34) requires a description of the density in terms of the pressure, which is obtained form the ideal gas law:

$$\frac{\rho}{M} = \frac{p}{RT}, \tag{7.36}$$

with M denoting the average molecular weight of the gas. Let $R_x = R/M_x$, with x denoting the dry and wet components respectively, then the substitution of Equation (7.36) in Equation (7.34) implies

$$\frac{dp}{p} = -\frac{g\,dh}{R_x\,T}. \tag{7.37}$$

This equation together with the assumption of an adiabatic atmosphere leads to a constant linear decay of the temperature as a function of height (see Appendix A):

$$\frac{dT}{dh} = -\alpha_0 = -9.75\ [^\circ\text{K/km}].$$

This means that an isolated atmosphere would develop such a profile, and that any temperature distribution with a smaller lapse rate is stable, while any distribution with a larger lapse rate is unstable, since the warmer air from below wants to flow to a higher altitude (inversion). The US Standard Atmosphere [11] assumes a constant lapse rate in the troposphere, more exactly at heights below 10 km[6]. The value specified by the US Standard Atmosphere is $\alpha = 6.5$ [°K/km], which implies a stable situation.

Integrating Equation (7.37) from h_0 to h leads to the barometric formula:

$$p(h) = p_0 e^{-\frac{1}{R_x}\int_{h_0}^{h} dh'\,\frac{g(h')}{T(h')}}, \tag{7.38}$$

which relates the pressure and the temperature. Using Equation (7.27) in (7.33), this implies the following expression for the tropospheric dry delay:

$$\Delta s_{z,d} = \kappa_1 \int_{h_0}^{h_s} dz\,\frac{p(z)}{T(z)} \tag{7.39}$$

with

$$\kappa_1 = 10^{-6}k_1, \qquad \kappa_2 = 10^{-6}k_2, \qquad \kappa_3 = 10^{-6}k_3,$$

denoting scaled versions of the refractivity constants. The remaining part is the art of evaluating these integrals. Hopfield [13] assumes a standard atmosphere

$$T(h) = T_0 - \alpha(h - h_0) = T_0\left(1 - \frac{h - h_0}{h_d}\right), \tag{7.40}$$

[6]The upper border of the troposphere is called *tropopause* and is defined as the altitude, where the temperature stops from falling at at constant rate. The tropopause is typically found at a height of 10 km.

with $h_d = T_0/\alpha$ being the scale height of the dry atmosphere. The assumption of a constant g allows to integrate the expression for the pressure:

$$p(h) = p_0 \left(\frac{T_0 - \alpha(h - h_0)}{T_0} \right)^{\mu+1} = p_0 \left(1 - \frac{h - h_0}{h_d} \right)^{\mu+1}, \tag{7.41}$$

with $\mu + 1 = g/(R_d\alpha)$. The numerical value of μ is 3.85, Hopfield uses the value $\mu = 4$. The result is used in Equation (7.39):

$$\begin{aligned} \Delta s_{z,d} &= \kappa_1 p_0 \frac{1}{T_0} \int_{h_0}^{h_d} dh \left(1 - \frac{h - h_0}{h_d} \right)^{\mu} \\ &\simeq 10^{-6} N_{0,d} \frac{h_d}{5}, \end{aligned}$$

with the approximation $h_0 \ll h_d$. Clearly integrating up to height h_d means that the temperature has dropped to 0°K, i.e. that all gases are frozen out. In reality the integration should be discontinued at the tropopause. Nevertheless, the model reproduces reality with a certain accuracy [13]. A similar model is used for the wet delay:

$$\Delta s_{z,w} \simeq 10^{-6} \left(k_2 \frac{e_0}{T_0} \frac{h_w}{5} + k_3 \frac{e_0}{T_0^2} \frac{h_w}{4} \right) \tag{7.42}$$

$$\simeq 10^{-6} N_{0,w} \frac{h_w}{5} \tag{7.43}$$

The assumption of a similar model for the wet delay is not too well justified, since the temperature profile is common to the wet and dry component, and thus does not allow for a different scale height for the dry and wet component. Nevertheless, the use of the mathematical analogy is found to typically match the experimental data reasonably well [13]. The assumption somehow models the phase transition of water vapor. The following numerical values are chosen for the scale heights of the wet and dry delay: $h_w = 12$ km and

$$h_d = 43.130 - 5.206 \sin^2 \phi \text{ [km]},$$

with ϕ being again the latitude. The interest of Hopfield's model is that it characterizes the zenith delay using the ground pressure of the dry gas and water vapor, as well as the temperature and two scale heights. Beyond the assumption of a constant lapse rate of the US Standard Atmosphere, Hopfield departs from it for altitudes that are above 10 km. Since only 10% of the gas is above that altitude, this might be considered acceptable for a first order model.

In 1972 Saastamoinen derived a more detailed model for the slant delay [14]. The derivation of this more complex model is deferred to Appendix B. The excess path length due to tropospheric propagation $\Delta s_x = c\Delta\tau_x$, expressed in meters is found to be (see [14] and Appendix B):

$$\begin{aligned} \Delta s_d &= \frac{0.002277}{\gamma \cos \zeta_0} (p_0 - \rho \tan^2 \zeta_0) \\ \Delta s_w &= \frac{0.002277}{\gamma \cos \zeta_0} \left(\frac{1255}{T_0} + 0.05 \right) e_0 \end{aligned}$$

The variable p_0, e_0, T_0, and ζ_0 denote the total and the partial water vapor pressures, the temperature, and the zenith angle at the user location, respectively. The pressures are measured in milibar, and the temperature in °K. ρ is a coefficient tabulated in Table 7.5, and γ is the correction of gravity described by Equation (7.35), evaluated at the height h_0, measured in kilometers, and latitude ϕ_0 of the receiver.

h	0	0.2	0.4	0.6	0.8	1	1.5	2	2.5	3	4	5	6
ρ	1.16	1.13	1.10	1.07	1.04	1.01	0.94	0.88	0.82	0.76	0.66	0.57	0.49

Table 7.5: Coefficients in Saastamoinen's expression for the dry excess path delay [14].

Research on modeling the troposphere is still on-going. GPS plays an increasingly important role in this context, since it reaches a comparable accuracy to radiosonde data but can be used much more extensively.

All of the above models require ground meteorological data, namely the partial pressures p_0 and e_0, as well as the temperature T_0. This information is not necessarily available. Blind models have therefore been developed. They use yearly averages instead of current data. One such model, called MOPS model, plays a crucial role in the context of WAAS augmentation. It is described in Section 14.7.3. A comparison of different data-driven and blind models was performed by Hornbostel and Hoque [16]. Their result is shown in Figure 7.12. The newest blind models of the ESA turn out to be nearly as good as the data-driven models described above. The accuracy is in the order of 5-10 cm. Higher accuracies require either the use of differential procedures or the determination of the zenith wet and/or dry delay, using an accurate mapping function, discussed next.

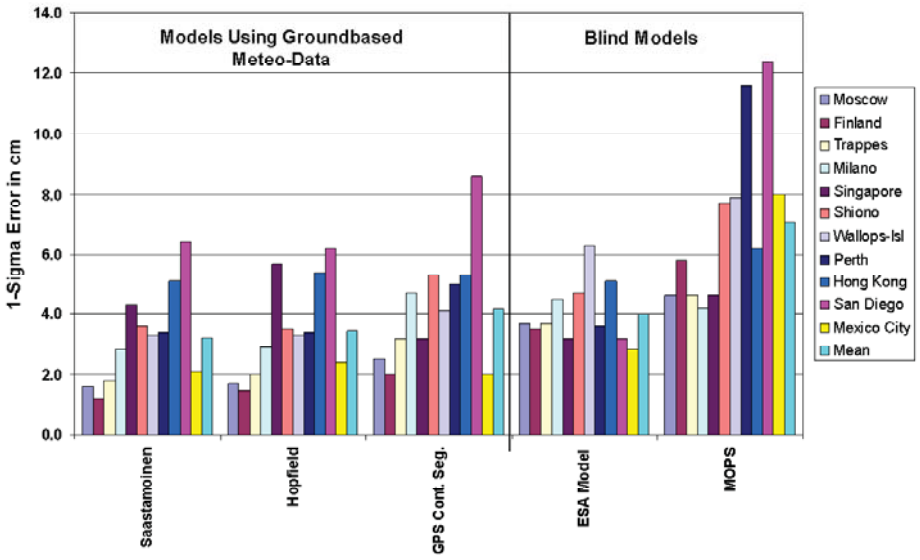

Figure 7.12: Comparison of different models for the tropospheric delay in the years 1980-1989 [Courtesy: A. Hornbostel, DLR [16]]

7.3.2 Mapping Functions - Tropospheric Delay

The mapping function for the dry delay is the quotient of the slant delay divided by the zenith delay:

$$m_d(E) = \frac{\displaystyle\int_{h_0}^{h} dz \, \frac{e^{-\frac{1}{R_d}\int_{h_0}^{z} dz' \, \frac{g(z')}{T(z')}}}{T(z)\cos\zeta'(z)}}{\displaystyle\int_{h_0}^{h} dz \, \frac{e^{-\frac{1}{R_d}\int_{h_0}^{z} dz' \, \frac{g(z')}{T(z')}}}{T(z)}}. \tag{7.44}$$

In the literature, it is common to express the mapping function in terms of the elevation $E = \frac{\pi}{2} - \zeta_0$. The Equations (7.44) and (7.32) fully specify the problem. Marini [17] as well as Davis, Herring, Shapiro, Rogers, and Elgered [18] have developed approximations in order to compute these functions. They are typically expanded into a partial fraction and truncated after a number of terms:

$$m_x(E) = \cfrac{1}{\sin E + \cfrac{a}{\sin E + \cfrac{b}{\sin E + c}}}, \tag{7.45}$$

or

$$m_x(E) = \cfrac{1}{\sin E + \cfrac{a}{\tan E + \cfrac{b}{\sin E + c}}}. \tag{7.46}$$

The parameters a, and b are functions of the pressures p_0, e_0 of the temperature T_0, of the temperature lapse rate α, and of the height of the tropopause h_t, which coincides with the height where the temperature stops decreasing. The temperature is assumed constant above that height, which is found to be acceptable, although not in accordance with the US Standard Atmosphere model. The second expression was introduced by Chao in order to ensure the convergence towards $1/\sin E$ for elevations approaching the zenith. It is an ad hoc choice, which turns out to provide a better fit. Details about such mapping functions are given in [18].

Rather then discussing these atmospheric modeling further, we shall provide a high level understanding for the particular form of the mapping function. That particular form has its origin in the curved surface of the earth. Consider an extremely simplified atmospheric model, with a spherical shell of height h in which the index of refraction is constant. In this case the path length ℓ in that shell is determined using the law of cosines:

$$2R_e\ell \sin E + \ell^2 = 2R_e h + h^2, \tag{7.47}$$

with $E = \pi/2 - \zeta$. This quadratic equation can be solved in closed form

$$\ell = -R_e \sin E + \frac{1}{2}\sqrt{4R_e^2 \sin^2 E + 8R_e h + 4h^2}. \tag{7.48}$$

The resulting mapping function $m(E)$ is plotted in Figure 7.13. The impact of earth curvature becomes significant at low elevations. Since tropospheric delays are in the order of 2 meters, the accuracy of mapping functions should be at the per mil level if they are to be used for carrier phase positioning. Alternatively, the solution can be expressed as a continued fraction. In that case, the mapping function $m(E) = \ell/h$ has the form of Equation (7.45), with a multiplier $1 + h/2R_e$, and coefficients $a = b = h/2R_e(1 + h/2R_e)$. Assuming that h is the height of the tropopause, and using the value of Davis et al. of 11.231 km, implies that $a = b = 0.0009$, which is close to the constant terms obtained by Davis.

The mapping functions of Marini and Davis et al. depend on atmospheric parameters on the ground, which need either to be measured or modeled. Niell for the first time introduced mapping functions that only depend on the latitude, height, and day of the year (DOY) [19]. Katsougiannopoulos, Pikridas, Rossikopoulos, Ifadis, and Fotiou [21] determined the accuracy of the Niell mapping function using radiosonde data, and found that it is at millimeter level for elevations

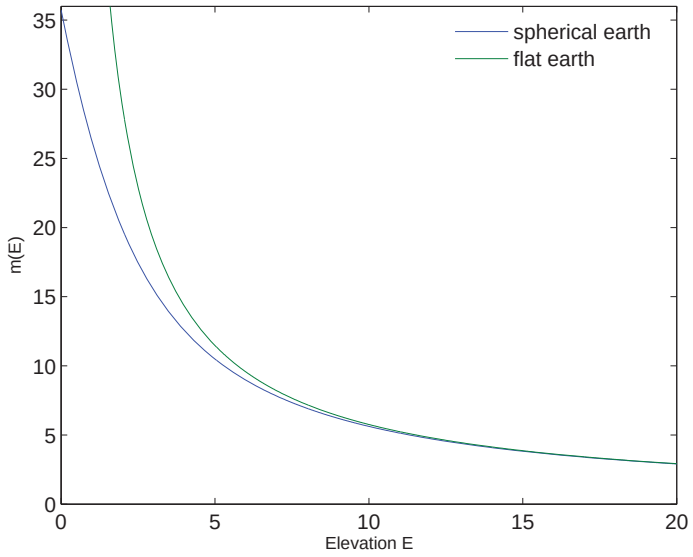

Figure 7.13: Mapping function for a homogeneous single layered troposphere in the case of a flat earth $m(E) = 1/\sin E$ and a spherical earth model as given by Equation (7.48).

above 30° and better than 2 cm for elevations above 20°. Niell's function reads [19][7]

$$f(E,a,b,c) = \frac{1+\dfrac{a}{1+\dfrac{b}{1+c}}}{\sin E+\dfrac{a}{\sin E+\dfrac{b}{\sin E+c}}}. \tag{7.49}$$

Let ξ represent any of the variables a, b, or c, then the coefficients ξ_d for the dry mapping expressed as a function of the latitude λ and of the day of the year t are given by:

$$\xi_d(\lambda,t) = \bar{\xi}_d(\lambda) - \Xi_d(\lambda)\cos\left(2\pi\frac{t-28}{365.25}\right). \tag{7.50}$$

The values of $\bar{\xi}_d(\lambda)$ and $\Xi_d(\lambda)$ are tabulated for $\lambda = 15°, 30°, 45°, 60°, 75°$, and interpolated linearly in-between (see Table 7.6). With these definitions, the dry mapping function becomes:

$$m_d(E,\lambda,h,t) = f(E,a_d(\lambda,t),b_d(\lambda,t),c_d(\lambda,t)) + h\left(\frac{1}{\sin E} - f(E,a_h(\lambda),b_h(\lambda),c_h(\lambda))\right), \tag{7.51}$$

with ξ_h being another set of three coefficients:

$$a_h = 2.53\cdot 10^{-5}, \qquad b_h = 5.49\cdot 10^{-3}, \qquad a_h = 1.14\cdot 10^{-3}.$$

The coefficients for the wet mapping are somewhat simpler. They do not require the consideration of the day of the year, i.e. $\Xi = 0$. The coefficients ξ_w are provided in Table 7.7. The wet mapping function reads:

$$m_w(E,\lambda,h) = f(E,a_w(\lambda),b_w(\lambda),c_w(\lambda)). \tag{7.52}$$

[7]The article was printed with a typographic error in the formula. The correct expression is found in Herring [20].

λ	15°	30°	45°	60°	75°
$\bar{a}_d$	$1.27699 \cdot 10^{-3}$	$1.26832 \cdot 10^{-3}$	$1.24654 \cdot 10^{-3}$	$1.21960 \cdot 10^{-3}$	$1.20460 \cdot 10^{-3}$
$\bar{b}_d$	$2.91537 \cdot 10^{-3}$	$2.91523 \cdot 10^{-3}$	$2.92884 \cdot 10^{-3}$	$2.90226 \cdot 10^{-3}$	$2.90249 \cdot 10^{-3}$
$\bar{c}_d$	$6.26105 \cdot 10^{-2}$	$6.28374 \cdot 10^{-2}$	$6.37218 \cdot 10^{-2}$	$6.38243 \cdot 10^{-2}$	$6.42584 \cdot 10^{-2}$
A_d	0	$1.271 \cdot 10^{-5}$	$2.652 \cdot 10^{-5}$	$3.400 \cdot 10^{-5}$	$4.120 \cdot 10^{-5}$
B_d	0	$2.141 \cdot 10^{-5}$	$3.016 \cdot 10^{-5}$	$7.257 \cdot 10^{-5}$	$1.172 \cdot 10^{-4}$
C_d	0	$9.013 \cdot 10^{-5}$	$4.350 \cdot 10^{-5}$	$8.479 \cdot 10^{-4}$	$1.704 \cdot 10^{-3}$

Table 7.6: Grid values of the coefficients needed for Niell dry mapping function. The interpolated values are used in Equation (7.50) to compute the coefficients for the mapping function provided by Equation (7.49). The coefficients must be computed with an accuracy of $\Delta a/a = 10^{-4}$, $\Delta b/b = 4 \cdot 10^{-4}$, and $\Delta c/c = 7 \cdot 10^{-4}$, for ensuring an accuracy of 1 mm at 3° [19].

λ	15°	30°	45°	60°	75°
a_w	$5.8021 \cdot 10^{-4}$	$5.6794 \cdot 10^{-4}$	$5.8118 \cdot 10^{-4}$	$5.9727 \cdot 10^{-4}$	$6.1641 \cdot 10^{-4}$
a_w	$1.4275 \cdot 10^{-3}$	$1.5138 \cdot 10^{-3}$	$1.4572 \cdot 10^{-3}$	$1.5007 \cdot 10^{-3}$	$1.7599 \cdot 10^{-3}$
c_w	$4.3472 \cdot 10^{-2}$	$4.6729 \cdot 10^{-2}$	$4.3908 \cdot 10^{-2}$	$4.4626 \cdot 10^{-2}$	$5.4736 \cdot 10^{-2}$

Table 7.7: Grid values of the coefficients needed for the Niell wet mapping function. The interpolated values are used the mapping function, i.e. Equation (7.49).

Niell obtained his results through extensive numerical simulation. The simulations are a combination of ray tracing and atmospheric modeling. The results of the simulations were then fitted to the mapping function using a least square algorithm.

7.3.3 Summary - Troposphere

The tropospheric delay T_d is the smaller of the atmospheric delays. Zenith delays are limited to $\sim$2.5 m. They can be described using blind models up to a variance of approximatively 12 cm. This is sufficient for a large number of applications. The tropospheric delay becomes a limiting factor in precision applications, however. The most promising approach in this context is using a mapping function in order to estimate the troposphere as two additional parameters.

Appendix A Adiabatic Atmosphere

The energy content of an ideal gas can be changed by supplying heat dQ or compressing the gas $-pdV$:

$$dU = dQ - p\,dV.$$

Let the gas be heated, while keeping the volume constant, then the change in energy is given by:

$$dU = C_v\,dT.$$

Thus

$$dQ = C_v\,dT + p\,dV.$$

In the adiabatic case, the system is isolated and there is no exchange of heat with the surrounding, i.e. $dQ = 0.$, i.e.:

$$p\,dV = -C_v\,dT.$$

Differentiating the ideal gas law, i.e. Equation (7.36) with $\rho = \nu M/V$, implies:

$$V\,dp + p\,dV = \nu R\,dT,$$

and substituting the above expression for $p\,dV$ as well as a little algebra leads to

$$\frac{dp}{p} = (1 + \frac{C_v}{\nu R})\frac{dT}{T}.$$

Equation (7.37) then implies the constant lapse rate:

$$dT = -\frac{gM_x}{R + \frac{C_v}{\nu}}\,dz = -\alpha_0\,dz,$$

which concludes the proof. Using the numerical values $g = 9.80665$, $M_x = 28.96$ [kg/kmol], $C_v/(\nu M_x) = 20.8$ [J/(mol·°K], $R = 8.314472$ [J/(mol·°K], this becomes

$$\alpha_0 = 9.75\ [°\mathrm{K/km}].$$

Appendix B Saastamoinen's Atmospheric Corrections

For the convenience of the reader, the present appendix describes the derivation of Saastamoinen. The notations are slightly adapted wrto the main text. We shall in particular omit obvious dependencies.

The model of the atmosphere used by Saastamoinen is based on a number of assumptions:

- Thayer's model of refractiviy holds.
- The gas is ideal.
- The atmosphere is homogenous, i.e. there is no azimuth dependency.
- The temperature is assumed to decay linearly in the troposphere, and to remain constant in the stratosphere. This is a refinement as compared to Hopfield, but still somewhat arbitrary.
- The earth is spherical. This becomes critical at elevations of less than 5°. At such elevations, the mismodeling of the atmosphere should be dominant, however.
- The gas pressure is zero above the stratopause, i.e. for $h \geq h_s$, which is reasonably well fulfilled, since 99% of the gas molecules are below.
- The partial pressure of the water vapor is zero above w, and the exponent of the decay is roughly a factor two faster than expected from the ration of the molecular weights of water and dry air.

The assumption that the temperature decreases with a constant rate in the troposphere and is constant in the stratosphere are strong simplifications. As shall be seen this only impacts a term that is zero in the zenith. The abnormal decay of the water pressure may be seen as a consequence of the phase transitions into droplets and ice crystals as soon as the temperature drops to 0°C.

In a first step, Saastamoinen derives an expression for the zenith angle $\zeta = \zeta(h)$ in terms of ζ_0. Remember that h_0 is the height at the receiver's location, and that $R_0 = R_e + h_0$ is the distance between that location and the center of the earth. Let h be the relative height of a gas volume under consideration, and let $R(h) = R_0 + h$ be the associated radius. Finally, let $n(h)$, and n_0 be the refraction index at the locations h and h_0, and define

$$y = \frac{n(h)R(h)}{n_0 R_0}$$

then Equation (7.31), which was derived using Snell's law, and the laws of sines implies:

$$\sin\zeta = \frac{1}{y}\sin\zeta_0,$$

and as is easily verified by trigonometry:

$$\begin{aligned}\frac{1}{\cos\zeta} &= \frac{y}{\cos\zeta_0}\left(1+\frac{y^2-1}{\cos^2\zeta_0}\right)^{-\frac{1}{2}} \\ &\simeq \frac{y}{\cos\zeta_0}\left(1-\frac{1}{2}\frac{y^2-1}{\cos^2\zeta_0}+\ldots\right)\end{aligned}$$

Since both $n(h)$ and n_0 are close to one, the following approximations can be used:

$$y = \frac{n(h)}{n_0}\left(1+\frac{z}{R_0}\right) \simeq 1+\frac{z}{R_0},$$

with $z = h - h_0$, and up to order z^2/R_0^2 :

$$y(y^2-1) \simeq 2\frac{z}{R_0}.$$

The above derivation describes the impact of the spherical earth while neglecting ray bending. Using these approximations, the slant $\Delta s = c\Delta\tau$ becomes:

$$\begin{aligned}\Delta s &= \int_{h_0}^{h_s} dz\,\frac{n(h)-1}{\cos\zeta(z)} \\ &= \frac{1}{\cos\zeta_0}\int_0^{z_s} dz\,(n(h)-1) - \frac{\tan^2\zeta_0}{R_0\cos\zeta_0}\int_0^{z_s} dz\,z(n(h)-1) \\ &=: \frac{1}{\cos\zeta_0}\Delta s_1 - \frac{\tan^2\zeta_0}{\cos\zeta_0}\Delta s_2,\end{aligned}$$

with $z_s = h_s - h_0 \simeq h_s$. Let p_d, e, and p denote the partial pressure of the dry gas, of the wet gas, and the total pressure of the gas, respectively, i.e.:

$$p = p_d + e.$$

Then using the Equations (7.27), and (7.28) implies that

$$\Delta s_1 = \kappa_1\int_0^{h_s} dz\,\frac{p_d}{T} + \kappa_2\int_0^{h_s} dz\,\frac{e}{T} + \kappa_3\int_0^{h_s} dz\,\frac{e}{T^2}. \tag{7.53}$$

The first integral in this expression also occurs in the computation of the density, as expressed by Equation (7.36):

$$\int_0^{h_s} dz\,\rho = \frac{1}{R_d}\int_0^{h_s} dz\,\frac{p_d}{T} + \frac{1}{R_w}\int_0^{h_s} dz\,\frac{e}{T} = \frac{p_0}{\bar{g}}, \tag{7.54}$$

with g denoting the gravitational acceleration in the center of mass of the atmospheric above the receiver:

$$\bar{g} = \frac{\int_0^{h_s} dz\,g(z)\rho(z)}{\int_0^{h_s} dz\rho(z)}. \tag{7.55}$$

Resolving Equation (7.54) for $\int dz\,p_d/T$ and using in Equation (7.53) leads to:

$$\Delta s_1 = \kappa_1\frac{R_d}{g}p_0 + \left[\kappa_2 - \kappa_1\frac{R_d}{R_w}\right]\int_0^{h_s} dz\,\frac{e}{T} + \kappa_3\int_0^{h_s} dz\,\frac{e}{T^2}. \tag{7.56}$$

Saastamoinen's approach is very judicious, since it does not need a model for the dry gas to determine Δs_1. It mostly relies on a water vapor model. The assumptions on the dry gas are that Thayer's law, the ideal gas law, and the constant lapse rate hold. The water vapor is concentrated in the troposphere. Similarly, to Equation (7.41), this implies

$$e(h) = e_0 \left(1 - \frac{z}{h_d}\right)^{\nu+1}.$$

with a different exponent due to the difference in the weight of the molecule of water vapor and dry gas:

$$\nu + 1 = \frac{g}{R_w \alpha} = \eta(\mu + 1),$$

and

$$\eta = \frac{R_d}{R_w} = \frac{M_w}{M_d}.$$

The ratio of the masses is roughly equal to 0.63. The upper limit of the integral w is chosen to be a height that is representative for the water vapor distribution. It is definitely not identical with Hopfield's scale height.

$$\begin{aligned}\int_0^w d\Delta h \, \frac{e}{T} &= \frac{e_0}{T_0} \frac{h_d}{\nu + 1} \left\{1 - \left(1 - \frac{w}{h_d}\right)^{\nu+1}\right\} \\ &= e_0 \frac{R_w}{g} \frac{1}{\eta} \left\{1 - \left(1 - \frac{w}{h_d}\right)^{\nu+1}\right\},\end{aligned}$$

and

$$\begin{aligned}\int_0^{h_w} d\Delta h \, \frac{e}{T^2} &= \frac{e_0}{T_0^2} \frac{h_d}{\nu} \left\{1 - \left(1 - \frac{w}{h_d}\right)^{\nu}\right\} \\ &= \frac{e_0}{T_0} \frac{1}{(g\eta/R_d - T_0/h_w)} \left\{1 - \left(1 - \frac{w}{h_d}\right)^{\nu}\right\}.\end{aligned}$$

This concludes the evaluation of Δs_1. The height w might be assumed to be around 4 km. Using Hopfield's scale height of ca. 43 km, this would imply that

$$\frac{R_d}{\eta} \left\{1 - \left(1 - \frac{w}{h_d}\right)^{\nu+1}\right\} \sim 0.4.$$

Saastamoinen uses $\eta = 4R_w/R_d$, and $w = h_d$. In this case, the above expression becomes 0.25. He justifies his choice with "substantial agreement with observed conditions during all seasons." The different thermodynamic phases of water: vapor, liquid droplets and ice crystals might be a cause for the discrepancy between theory and experimental evidence.

The evaluation of Δs_2 requires a model for the total pressure p. Since the integrand

$$\left(1 - \frac{z}{h_d}\right)^{\mu} z$$

has its maximum at $z = h_d/(\mu + 1) \simeq 10$ [km], the dry component will dominate, and the model can be simplified accordingly.

In the lower part of the atmosphere, the model again assumes a constant lapse rate (adiabatic condition), while it supposes an isothermal behavior in the the upper part, i.e. the temperature is constant there. The US Standard Atmosphere defines a constant temperature between 10 and 20 km. Above this altitude direct heating from the sun is more and more pronounced, reaching

a maximum at around 80 km, where ionization starts becoming relevant. The model is thus an oversimplification. Due to the low prevalent pressure at these altitudes these simplifications are expected to be less impacting than the simplifications made at lower altitudes. The constancy of temperature is equivalent to an exponential decay of the pressure as a function of height. The integral Δs_2 is split into two contribution, one from the user's height to the tropopause height h_t, which is denoted by $\Delta s_{2,1}$ and one which covers the heights above, denoted by $\Delta s_{2,2}$:

$$\begin{aligned}\Delta s_2 &= \frac{1}{R_0}\int_0^{h_t} dz(n-1)z + \frac{1}{R_0}\int_{h_t}^{h_s} dz(n-1)z \\ &= \Delta s_{2,1} + \Delta s_{2,2}.\end{aligned}$$

The integral $\Delta s_{2,1}$ is evaluated through an integration by parts and by substituting back the definitions of p_t, p_0, n_t and n_0:

$$\begin{aligned}\Delta s_{2,1}(h_t) &= \frac{1}{R_0}\int_0^{h_t} dz\,(n-1)z \\ &= \frac{1}{R_0}\kappa_1\frac{p_0}{T_0}\int_0^{h_t} dz\,\left(1-\frac{z}{h_d}\right)^{\mu} z \\ &= \frac{1}{R_0}\kappa_1\frac{p_0}{T_0}\left[-\frac{h_d}{\mu+1}\left(1-\frac{h_t}{h_d}\right)^{\mu+1} h_t - \frac{h_d^2}{(\mu+1)(\mu+2)}\left\{\left(1-\frac{h_t}{h_d}\right)^{\mu+2}-1\right\}\right] \\ &= \frac{1}{R_0}\left(-\frac{R_d}{g}(n_t-1)T_t h_t - \frac{R_d^2}{g^2(1+\alpha R/g)}\left[(n_t-1)T_t^2-(n_0-1)T_0^2\right]\right).\end{aligned}$$

The integral $\Delta s_{2,2}$ needs an expression for $p(z)$ in the case of a constant temperature $T(z) = T_t$. The latter is obtained from Equation (7.38):

$$p(h) = p_t \exp\left(-\frac{\gamma}{T_t}(h-h_t)\right),$$

with $\gamma = g/R_d$. The desired expression for $\Delta s_{2,2}$ can be obtained as a limiting case:

$$p(h) = p_t \lim_{\alpha\to 0}\left(1-\beta\frac{\gamma}{T_t}(h-h_t)\right)^{\frac{1}{\beta}},$$

and since the limit is reached monotonically in β, the integration process and the limit can be exchanged. Alternatively, one might just compute the result directly. In either cases:

$$\begin{aligned}\Delta s_{2,2} &= \frac{1}{R_0}\int_{h_t}^{h_s} dz\,(n-1)z \\ &= -\frac{R_d}{gR_0}(n_s-1)T_s h_s - \frac{R_d^2}{g^2 R_0}(n_s-1)T_s^2 \\ &\quad + \frac{R_d}{gR_0}(n_t-1)T_t h_t + \frac{R_d^2}{g^2 R_0}(n_t-1)T_t^2.\end{aligned}$$

Since the temperature is assumed to be constant between h_t and h_s, the identity $T_s = T_t$ holds. Furthermore, Equations (7.27) and (7.38) lead to the relation:

$$\begin{aligned}n_s - 1 &= \kappa_1\frac{p_s}{T_s} \\ &= \kappa_1\frac{p_t e^{-\gamma(h_s-h_t)/T_t}}{T_t} \\ &= (n_t-1)e^{-\gamma(h_s-h_t)/T_t},\end{aligned}$$

which implies that $n_s - 1 \ll n_t - 1$. Neglecting the smaller terms, leads to a simplified expression for:

$$\Delta s_{2,2} = \frac{R_d}{gR_0}(n_t - 1)T_t h_t + \frac{R_d^2}{g^2 R_0}(n_t - 1)T_t^2.$$

and thus also to a simplified expression for:

$$\Delta s_2 = \frac{R_d^2}{g^2 R_0} \frac{(n_0 - 1)T_0^2 + \alpha \frac{R_d}{g}(n_t - 1)T_t^2}{1 + \alpha \frac{R_d}{g}}.$$

Using the expression for the refractivity (Equation (7.27)), as well as the expressions for the temperature and pressure in the troposphere (Equations (7.40) and (7.41)) leads to:

$$\begin{aligned} \Delta s_2 &= \kappa_1 \frac{R_d^2}{g^2 R_0} \frac{p_0 T_0 + \alpha \frac{R_d}{g} p_t T_t}{1 + \alpha \frac{R_d}{g}} \\ &= \kappa_1 \frac{R_d^2}{g^2 (R_e + h_0)} \frac{1 + \alpha \frac{R_d}{g}(1 - \frac{h_t}{h_d})^{\frac{g}{R_d \alpha} + 1}}{1 + \alpha \frac{R_d}{g}} p_0 T_0 \\ &= \tilde{\rho}(h_0) p_0 T_0. \end{aligned}$$

The height of the troposphere h_t, as well as the scale height associated with the constant lapse rates can be seen as constants of the model. Thus the factor $\tilde{\rho}(h_0)$ could be considered to be a function of h_0 only. Surprisingly, Saastamoinen considers $\rho(h_0) = \tilde{\rho}(h_0) p_0 T_0$ to be a function of h_0 only. The dependency on pressure and temperature are neglected. Finally, the gravity constant $\bar{g}$ needs to be determined. This is done using the identity (see Chapter 9):

$$g(h) = g_0 \left(1 - 0.0026 \cos\phi - 0.0031h\right).$$

with

$$g_0 = 9.80655 \ [\mathrm{m/s^2}].$$

This implies that

$$\bar{g} = g_0(1 - 0.0026 \cos\phi - 0.0031\bar{h})$$

with

$$\bar{h} = \frac{\int_{h_0}^{h_s} dh\, \rho(h) h}{\int_{h_0}^{h_s} dh\, \rho(h)} = \frac{\int_{h_0}^{h_s} dz\, (n-1)(z + h_0)}{\int_{h_0}^{h_s} dz\, (n-1)} = \frac{\Delta s_2}{\Delta s_1}.$$

The latter identities are approximations, which become exact if $\kappa_1 = \kappa_2$, and the $\kappa_3 = 0$. Saastamoinen indicates an expression that is consistent with experimental data[8]:

$$\bar{h} = 0.73 + 0.9h_0.$$

This expression finally implies that

$$\bar{g} = 9.784(1 - 0.0026 \cos\phi - 0.0028h_0).$$

The numerical evaluation of the above equations finally leads Saastamoinen to his expressions for the dry and wet delay. Some possible slight improvements of these expressions have been discussed.

[8]The offset of 7.3 km in [14] must be a typographic error.

Exercises

1. Derive Snell's law, i.e. Equation (7.5), from Fermat's principle.
2. Determine the ionospheric delay from pseudorange measurements at the Galileo frequencies E1 at $154 \cdot 10.23$ MHz, and E5a at $115 \cdot 10.23$ MHz. Indicate a linear combination of such measurements which does not depend on the first order tropospheric delay.
3. Indicate a linear combination that eliminates both the first and second order delay.
4. Compute the relation between the group and phase delay for the first and second order ionospheric correction.
5. Can all of the above combinations for pseudorange measurements also be used for phase measurements? Indicate the suitable ones.

Bibliography

[1] J. Christie, B. Parkinson, P. Enge, "The Effect of the Ionosphere and C/A Frequency on GPS Signal Shape: Considerations for GNSS2," *Proc. ION GPS '96,* pp. 647-653, 1996.

[2] G. Gao, S. Datta-Barua, T. Walter, P. Enge, "Ionosphere Effects for Wideband GNSS Signals," *Proc. Annual Meet. ION'07,* pp. 147-155, 2007.

[3] P. Henkel, G. Gao, T. Walter, C. Günther, "Robust Vector Phase Locked Loop for Wideband Signals," *submitted ENC-GNSS 2009.*

[4] J.A. Klobuchar, "Ionospheric Effects on GPS," in *Global Positioning System, Theory and Applications,* vol. I, pp. 485-515, AIAA, Washington DC, 1996.

[5] *GPS Interface Control Document*, GPS-ICD200C
`http://www.navcen.uscg.gov/pubs/gps/icd200/icd200cw1234.pdf`

[6] N. Jakowski, M.M. Hoque, C. Mayer, "A New Global TEC Model for Estimating Transionospheric Radio Wave Propagation Errors," *J. of Geodesy,* vol. 85, pp. 965-974, 2011.

[7] M.M. Hoque, N. Jakowski, "Higher Order Effects in Precise GNSS Positioning," *J. of Geodesy,* vol. 81, pp. 259-268, 2007.

[8] S. Bassiri, G.A. Hajj, "Higher-Order Ionospheric Effects on the Global Positioning Systems Observables and Means of Modelling them," *Manuscripta Geodetica,* vol. 18, pp. 280-289, 1993.

[9] B. Nava, P. Coïsson, S.M. Radicella, "A New Version of the NeQuick Ionosphere Electron Density Model," *J. of Atm. and Solar-Terrestrial Phys.,* vol. 70, pp. 1856-1862, 2008.

[10] J.J. Spilker Jr., "Tropospheric Effects on GPS," in *Global Positioning System, Theory and Applications,* vol. I, pp. 517-546, AIAA, Washington DC, 1996.

[11] *US Standard Atmosphere 1976,* NOAA, NASA, USAF, Washington D.C., 1976.

[12] G.D. Thayer, "An Improved Equation for the Radio Refractive Index of Air," *Radio Sci.,* vol. 9, pp. 803-807, 1974.

[13] H.S. Hopfield, "Two-Quartic Tropospheric Refractivity Profile for Correcting Satellite Data," *J. of Geophysical Res.,* vol. 74, pp. 4487-4499, 1969.

[14] J. Saastamoinen, "Atmospheric Correction for the Troposphere and Stratosphere in Radio Ranging of Satellites," in *The use of Artificial Satellites for Geodesy, Geophys. Monogr., AGU* vol. 15, pp. 247-251, 1972.

[15] RTCA, "Minimum Operational Performacne Standards for Global Positioning System/Wide Areas Augementation System Airborn Equipment," RTCA/DO-229C, 2001.

[16] A. Hornbostel, M. Hoque, "Analysis of Tropospheric Correction Models for Local Events within the GSTB Test Case APAF," *Proc. ION GNSS 2004*, pp. 902-914, 2004.

[17] J.W. Marini, "Correction of Satellite Tracking Data for an Arbitrary Tropospheric Profile," *Radio Sci.,* vol. 7, pp. 223-231, 1972.

[18] J.L. Davis, T.A. Herring, I.I. Shapiro, A.E.E. Rogers, G.Elgered, " Geodesy by Radio Interferometry: Effects of Atmospheric Modeling Errors on Estimates of Baseline Length," *Radio Sci.,* vol. 20, pp. 1593-1607, 1985.

[19] A.E. Niell, "Global Mapping Functions for the Atmosphere Delay at Radio Wavelengths," *J. Geophys. Res.,* vol. 101, pp. 3227-3246, 1996.

[20] T.A. Herring, "Modelling Atmospheric Delays in the Analysis of Space Geodetic Data," in *Proc. Symp. on Refraction of Transatmospheric Signals in Geodesy,* NL Geod. Comm. Ser. 36, Ed. J.C. De Munck, T.A.Th. Spoelstra, pp. 157-164.

[21] S. Katsougiannopoulos, C. Pikridas, D. Rossikopoulos, I.M.'Ifadis, A. Fotiou, "Tropospheric Refraction Estimation Using Various Models, Radiosonde Measurements and Permanent GPS Data," *Proc. XXIII FIG Congress,* Munich, Oct. 8-14, 2006.